



JGR Planets

RESEARCH ARTICLE

10.1029/2024JE008832

Key Points:

- The global distribution of Bouguer anomalies in craters are mapped as regions in which hydrothermal circulation was a dominant process
- Novel joint inversions allow us to regionally investigate density and magnetization signatures within such craters
- A dominant lack of magnetization signatures likely indicates an inactive dynamo at times in which hydrothermal circulation was still active

Supporting Information:

Supporting Information may be found in the online version of this article.

Correspondence to:

A. Mittelholz, anna.mittelholz@eaps.ethz.ch

Citation:

Mittelholz, A., Moorkamp, M., Broquet, A., & Ojha, L. (2025). Gravity and magnetic field signatures in hydrothermally affected regions on Mars. *Journal of Geophysical Research: Planets*, 130, e2024JE008832. https://doi.org/10.1029/2024JE008832

Received 14 NOV 2024 Accepted 26 MAR 2025

Author Contributions:

 ${\bf Conceptualization:}\ {\bf Anna}\ {\bf Mittelholz},$

Lujendra Ojha

Data curation: Anna Mittelholz,

Adrien Broquet

Formal analysis: Anna Mittelholz, Adrien Broquet, Lujendra Ojha Methodology: Max Moorkamp Visualization: Anna Mittelholz Writing - original draft: Anna Mittelholz

Writing – review & editing:
Adrien Broquet, Lujendra Ojha

© 2025. American Geophysical Union. All Rights Reserved.

Gravity and Magnetic Field Signatures in Hydrothermally Affected Regions on Mars

Anna Mittelholz¹, Max Moorkamp², Adrien Broquet^{3,4}, and Lujendra Ojha⁵

¹Department of Earth and Planetary Sciences, ETH Zurich, Zurich, Switzerland, ²Technische Universität Berlin, Institut für Angewandte Geowissenschaften, Berlin, Germany, ³Lunar and Planetary Laboratory, University of Arizona, Tucson, AZ, USA, ⁴Now at Institute for Planetary Research, German Aerospace Center, DLR, Berlin, Germany, ⁵Department of Earth and Planetary Sciences, Rutgers University, New York, NJ, USA

Abstract Multiple lines of evidence indicate that liquid water-rock interactions occurred on ancient Mars, particularly within the crust, where hydrothermal systems have been hypothesized. Such hydrothermal circulation (HC) can significantly lower temperatures in the crust, thereby restricting the viscoelastic relaxation of impact craters. Craters with minimal relaxation are characterized by their large depth-to-diameter ratio and prominent Bouguer gravity anomalies. Additionally, HC can induce magnetic anomalies through chemical remanent magnetization (CRM). Consequently, if HC was widespread on Mars, the gravitational signatures of unrelaxed craters may correlate with their magnetic signatures. To investigate how HC influenced the magnetic characteristics of the Martian crust, we focus on the region surrounding several unrelaxed craters in the southern highlands, where hydrothermal activity was likely prevalent. We use a newly developed joint inversion approach and model magnetization and density in such regions to investigate how hydrothermal systems affect those parameters. The inversion approach makes use of a mutual information term in which models with a parameter relationship are favored, that is, models in which magnetization and density distributions are correlated. Despite showing large Bouguer gravity anomalies and forming over 3.75 billion years ago, when the Martian dynamo was most likely active, investigated craters and surrounding regions exhibit minimal magnetic anomalies. We propose that this lack of magnetic signatures is most likely due to demagnetization of the crust through CRM, induced by HC long after the Martian dynamo ceased. Our findings suggest that deep, long-lived hydrothermal systems—likely fueled by heat-producing elements—were present, potentially creating habitable conditions on early Mars.

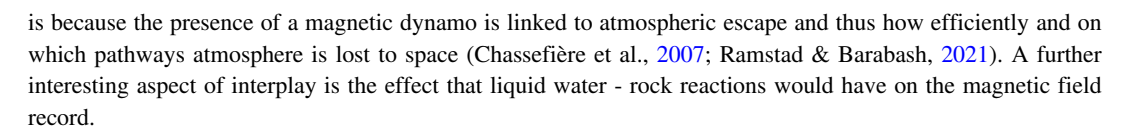
Plain Language Summary Ancient Mars has been shown to have hosted liquid water on the surface, but also within the crust in the form of active hydrothermal systems. Accelerated crustal cooling due to circulating crustal water after impacts can lead to pronounced gravity anomalies because the crust does not have time to fully relax. Such gravity anomalies can thus serve as proxy to identify regions where hydrothermal alteration was active at the time of the impact. Because water-rock interactions also lead to magnetic signatures by forming magnetite as an alteration product, one would expect such regions to exhibit magnetic field signatures. Here, we focus on regions in which hydrothermal systems were likely active to investigate magnetization and density variations. Using unrelaxed craters as proxy, we find that such regions are distributed along the dichotomy and are collocated with morphological and mineralogical indicators for water activity. In those regions, hydrothermal alteration was likely active for longer than the Martian dynamo and affected large portions of the crust. Thus, our results indicate long-lasting and deep hydrothermal alteration, suggesting favorable conditions for habitable environments on early Mars, temporally and spatially.

1. Introduction

1.1. Water and Crustal Magnetization on Mars

Mars was once a much more habitable world. Morphological features, such as valley networks, show unequivocal signs of water on the surface. These are remnants of fluvial and/or glacial activity (e.g., Grau Galofre et al., 2020; Hynek et al., 2010) likely under fluctuating climatic conditions (Wordsworth et al., 2021). In addition, the mineralogical record provides evidence for rock alteration in the presence of water (e.g., Carter et al., 2015; Ehlmann et al., 2011). The exact timing of climate events is not well constrained; however, peak fluvial activity is ascribed to the late Noachian and early Hesperian, 3.5 to 3.7 Ga (Ga = billion years ago) (Fassett & Head, 2008). Additionally, we note that the planetary-scale magnetic field directly influences the climatic state of a planet. This

MITTELHOLZ ET AL. 1 of 19



Today, Mars has no active dynamo field, but strongly magnetized crustal rock indicates that it once operated, likely since early Martian history, ~4.5 Ga (e.g., Acuña et al., 1999; Lillis et al., 2013; Mitteholz & Johnson, 2022; Mittelholz et al., 2020). The latest evidence for a dynamo at 3.7 Ga is derived from the crustal magnetic field record of Lucus Planum, a pyroclastic flow unit (Mitteholz & Johnson, 2022; Mittelholz et al., 2020; Ojha & Mittelholz, 2023). The paleomagnetic record provided by the Martian meteorite ALH 84001 (Steele et al., 2023) further puts constraints on an active dynamo at 4.1 and 3.9 Ga. Thus, a long-lived dynamo from 4.5 Ga to at least 3.7 Ga is possible (Mittelholz et al., 2024; Steele et al., 2024), but interruptions in dynamo activity cannot be ruled out. Either way, the timing of liquid water activity on the Martian surface coincides with an active dynamo.

As a result, the Martian crustal magnetic field record might be related to a process called chemical remanent magnetization (CRM) (Chassefière et al., 2013; Quesnel et al., 2009; Scott & Fuller, 2004). CRM arises from chemical processes such as magnetic mineral creation, modification of the oxidation state, phase changes, and the growth of magnetic minerals within the crust at temperatures below the Curie point of the rock's magnetic carriers, and in the presence of an external magnetic field. A notable geological process responsible for CRM on Earth is serpentinization, a high-temperature fluid-rock reaction that typically occurs in ultramafic rocks of oceanic crust (Toft et al., 1990), ophiolites (Bonnemains et al., 2016), and in ultramafic intrusions (He et al., 2016). The serpentinization process leads to the oxidation of ferrous minerals (poor magnetic carriers) into Fe³⁺ rich serpentines and magnetite (Andreani et al., 2013), which are considered the most significant cause of remanent magnetization in crustal rocks on Earth (Dunlop & Özdemir, 2001) and possibly Mars (Dunlop & Arkani-Hamed, 2005). As a magnetic grain produced by serpentinization below its Curie point grows through a critical volume, its magnetic moment becomes blocked, that is, it acquires a CRM.

Hence, the presence of liquid water on Mars during the Noachian might have played an important role in creating the observed magnetization. In the presence of a magnetic field, CRM reactions would have led to magnetization in the direction of the external (dynamo) field. Alteration or crystallization in the absence of a field would have in turn demagnetized crust, that is, magnetic carriers would be magnetized with random directionalities (due to a lacking directing dynamo field) resulting in net zero magnetization.

This leads to the question, which regions on Mars would have been affected by water-rock interactions, and more importantly, mechanisms leading to CRM? In general, a broad spatial correlation between valley networks and the crustal magnetic field has been noted (Harrison & Grimm, 2002). However, given the general increased geological activity in the Noachian and early Hesperian, the question arises if this correlation is in fact due to water-related processes or collocated due to similar timing of events. Further, surface runoff leading to valley networks might have been short-lasting, surficial, and thus not an efficient mechanism for described alteration processes. On the other hand, catchment areas with longer lasting water interaction are more likely to host alteration processes, but those have a relatively small spatial footprint (Goudge et al., 2021) likely below or at the level of currently resolvable magnetic field signatures (maximum global resolution: ~130 km). In addition, alteration is generally more efficient in low-to-mid temperature environments. On Earth it is typically observed along the mid-oceanic ridge (Mével, 2003), where CRM provides a mechanism for magnetizing crustal rock (Draeger et al., 2006). This suggests that instead of focusing on regions in which surface water was likely active, one should focus on regions in which indications for subsurface, crustal water and hydrothermal activity exist.

1.2. Hydrothermal Systems on Mars

Hydrothermal circulation has been proposed to occur on Mars. The three main ingredients necessary for hydrothermal circulation and serpentinization are: olivine-rich ultramafic rocks (e.g., Edwards et al., 2008; Hamilton & Christensen, 2005; Ody et al., 2013), liquid water (e.g., Ehlmann & Edwards, 2014), and high surface heat flows (Ojha et al., 2021; Plesa et al., 2016). All of those were readily available on Mars during the Noachian, when the majority of the crustal magnetization is postulated to have been acquired.

Groundwater interactions with magma in Elysium Planitia are thought to have formed the Athabasca Valley outflow system (Keszthelyi et al., 2007; Miller et al., 2024). The highly altered nature of the Martian crust

MITTELHOLZ ET AL. 2 of 19



(Lognonné et al., 2020) further suggests that groundwater circulation could have extended to great depths (>10s km; Clifford, 1993; Hanna & Phillips, 2005). Recently, abundant intra-crustal water at 10–11 km was shown to be a possible, although debated (Jakosky, 2025), scenario based on InSight seismic data in combination with rock physics models (Wright et al., 2024). Additional evidence of serpentinization in the deep crust is provided by the spectral detection of minerals associated with serpentinization across the Noachian highlands, particularly within impact basins, through the uplift of deep crustal rocks (Amador et al., 2018; Carter et al., 2013).

Several studies suggest that in the presence of groundwater, heat from various sources could have led to conditions favorable for hydrothermal activity, including impacts (Osinski et al., 2013), magmatism (Harrison & Grimm, 2002), or radiogenic elements (Ojha et al., 2021). Furthermore, H₂ is released in the serpentinization process and the released H is then lost to space. Chassefière et al. (2013) demonstrate that a significant portion of the water present on early Mars may have been sequestered in subsurface serpentine through serpentinization, also contributing to atmospheric loss and shaping Mars' geochemical and isotopic evolution. Additionally, Bultel et al. (2025) recently modeled the required magnetite abundance to explain observed magnetic field strengths and then simulated magnetite production through aqueous alteration of various Martian rock compositions using a thermodynamic model. Their findings suggest that serpentinization of dunite at low water-to-rock ratios could account for even the strongest anomalies, while alteration of shergottites and pyroxenites at higher ratios could explain weaker anomalies. Thus, hydrothermal circulation and subsequent serpentinization of the Martian crust and subsequent CRM may have been a key contributor to the strong magnetic anomalies on Mars (Quesnel et al., 2009; Scott & Fuller, 2004).

Having established that hydrothermal alteration was likely an important process - how can we identify affected regions to be further investigated? While the location of a surface drainage system is observable, signs of hydrothermal activity are more difficult to identify. However, a likely location for long-lasting hydrothermal systems has been proposed in places where excess subsurface mass, that is, positive Bouguer gravity anomalies, are associated with craters. While craters usually relax viscoelastically and become isostatically compensated over time, some observed dominant Bouguer gravity signatures are thought to result from accelerated cooling of the crust subsequent to the impact, which hinders relaxation (Mohit & Phillips, 2007). Accelerated cooling can be facilitated by the presence of hydrothermal systems (Parmentier & Zuber, 2007), resulting in efficient heat transport due to the water circulation and thus limited relaxation of the crust. Parmentier and Zuber (2007) show the effect of increasing water circulation in the crust and the associated decreasing effect of the relaxation rate over time to explain preservation of ancient and sharp crustal thickness variations. Long-lived heat producing elements (HPEs) have been proposed as potential energy source for sustaining active hydrothermal systems over geological time scales over 100–1,000 Ma (Ojha et al., 2021). In that framework, the lack of relaxation would lead to a mass surplus associated with uplifted mantle material, leaving the basin in a state of superisostasy. Specifically in the Eridania basin, for craters such as Newton and Copernicus, pronounced Bouguer anomalies within the crater interior have been observed and mineralogical and morphological properties in the region corroborate the hypothesis that the location was affected by hydrothermal alteration (Oiha et al., 2021). Typically, such regions also show craters with high depth-to-diameter ratios, also due to the effect of a quickly cooling crust and limited crustal relaxation. Regions with active hydrothermal alteration can thus be identified in the gravity record and provide ideal locations for investigating the effect of water-rock interactions on observed magnetic signatures.

1.3. 3D Geophysical Modeling of the Crust

Satellite data have been used to model the crustal magnetic field of Mars (e.g., Langlais et al., 2019; Mittelholz et al., 2018; Morschhauser et al., 2014). Magnetization models can be derived from magnetic field models (e.g., Vervelidou et al., 2017) or are a direct product of the inversions (e.g., Langlais et al., 2019), where the estimated quantity is the dipole moment from which magnetization is derived. In both cases, a layer thickness has to be assumed, typically a 40 km thick crust. Solving for 3D crustal magnetization is highly non-unique and the satellite data record does not allow for such robust models. Here, we present a first attempt to address this issue, by including a further source of information on the crust, the gravity field. In the inversion, we jointly evaluate magnetization and density from these data sets. Because no physical relationship exists for varying magnetization and density distributions (e.g., Blakely, 1996), we propose a method that is driven by matching parameter relationships (Moorkamp, 2021). As such, the models aim to describe all individual data sets by minimizing the

MITTELHOLZ ET AL. 3 of 19



misfits between data and model (with their respective regularization terms) in addition to favoring solutions that lead to parameter relationships between the models, that is, the coupling. Because CRM reactions should affect both density and magnetization compared to surrounding material, this method is particularly suitable in representing Martian 3D crustal magnetization and density for the first time.

In this study, we globally identify craters exhibiting notable superisostatic Bouguer gravity anomalies, which we interpret as the result of accelerated crustal cooling driven by hydrothermal circulation. We perform joint inversions of observed gravity and magnetic anomalies to constrain the subsurface properties in identified regions. This joint analysis sheds light on possible correlations between the gravity and magnetic field, constrains 3D crustal structure, and allows unraveling the investigated craters' hydrothermal and evolutionary history. We introduce data and models used for the analysis in Section 2 and describe the methods used in Section 3. Section 4 presents a global analysis of Bouguer gravity signatures to identify regions of interest followed by a more detailed analysis facilitated by regional joint inversions. Lastly, in Section 5 we provide a discussion of our results and provide recommendations on possible future geophysical investigations that could enhance presented models.

2. Data

The main input data for this study consist of three components of a magnetic field model and the gravity signal associated with the local crustal structure which we aim to investigate.

Magnetic data are extracted from a global crustal magnetic field model (Langlais et al., 2019) to avoid contamination from external magnetic field sources that may affect individual data tracks. We use spherical harmonic coefficients and evaluate two random data points per horizontal bin of 60×60 km from two different altitudes, 130 and 200 km for all three components of the magnetic field. Because the input model incorporates Mars Atmosphere and Volatile Evolution (MAVEN; Jakosky et al., 2015) and Mars Global Surveyor (MGS; Acuña et al., 1999) data with nearly global coverage down to those altitudes (Mitteholz & Johnson, 2022), we consider the model to be stable and to provide best available resolution while not introducing artifacts from downward continuation.

Gravity anomalies originate from multiple sources, including relief variations at the top and base of the crust. Classical crustal thickness inversions assume that observed Bouguer anomalies (i.e., topography-corrected free-air gravity) originate solely from relief variations at the base of the crust (Wieczorek et al., 2022). For the identification of unrelaxed craters, we thus use Bouguer anomalies which allow to identify signatures associated with the crust-mantle interface. For our joint inversion of the gravity and magnetic field, however, we are interested in density variations within the crust. To highlight intra-crustal density variations, we remove long-wavelength gravity anomalies associated with the crust-mantle interface and isolate the gravity signal coming from short-wavelength anomalies.

We use the GMM3 spherical harmonic model of the gravitational potential (Genova et al., 2016). From the observed free air gravity we subtract gravity contributions from (a) surface topography and (b) modeled relief of the base of the crust. This is achieved by computing the Bouguer correction using topography data from Mars Orbiter Laser Altimeter (MOLA) topography (MarsTopo2600 model of Wieczorek (2015)) and forward modeling the gravity originating from the crust-mantle relief model of Wieczorek et al. (2022), which assumes an average crustal thickness of 57 km, density of $2,800 \text{ kg m}^{-3}$ and a degree-50 half wavelength downward continuation filter. These calculations use the DSP package of Broquet (2024). The result is a map of short-wavelength gravity anomalies that we assume to be mostly unrelated to crustal thickness variation and rather originate from crustal density anomalies (as discussed for the Moon by Jansen et al. (2017)). In the following, we will refer to this pre-processed data set for the inversion as residual gravity data, while the topography-corrected data will be referred to as Bouguer gravity and used for the identification of unrelaxed craters as a proxy for hydrothermal activity.

For the inversion discussed in the next section, we assign uncertainty of magnetic and residual gravity data of 1 nT and 1 mGal. These uncertainties are low, but justified because, in the case of magnetic data, the use of a crustal field model ensures that the input data are not contaminated, for example, by fields of ionospheric origin and the model will have extracted crustal field information as well as possible. For residual gravity, we use data up to degree 90, which corresponds to the degree strength and signal-to-noise ratio of 1 that however drops off significantly for longer wavelengths. We thus assign 1 mGal uncertainty to the residual gravity field. While these uncertainties affect the RMS misfit value of the final model, assessment of appropriate fit is done by visually

MITTELHOLZ ET AL. 4 of 19

xxm/doi/10.1029/2024E008832 by Disch Zentrum F. Luft-U. Raum Fahrt In D. Helmholtz Gemein., Wiley Online Library on [07/10/2025]. See the Tern

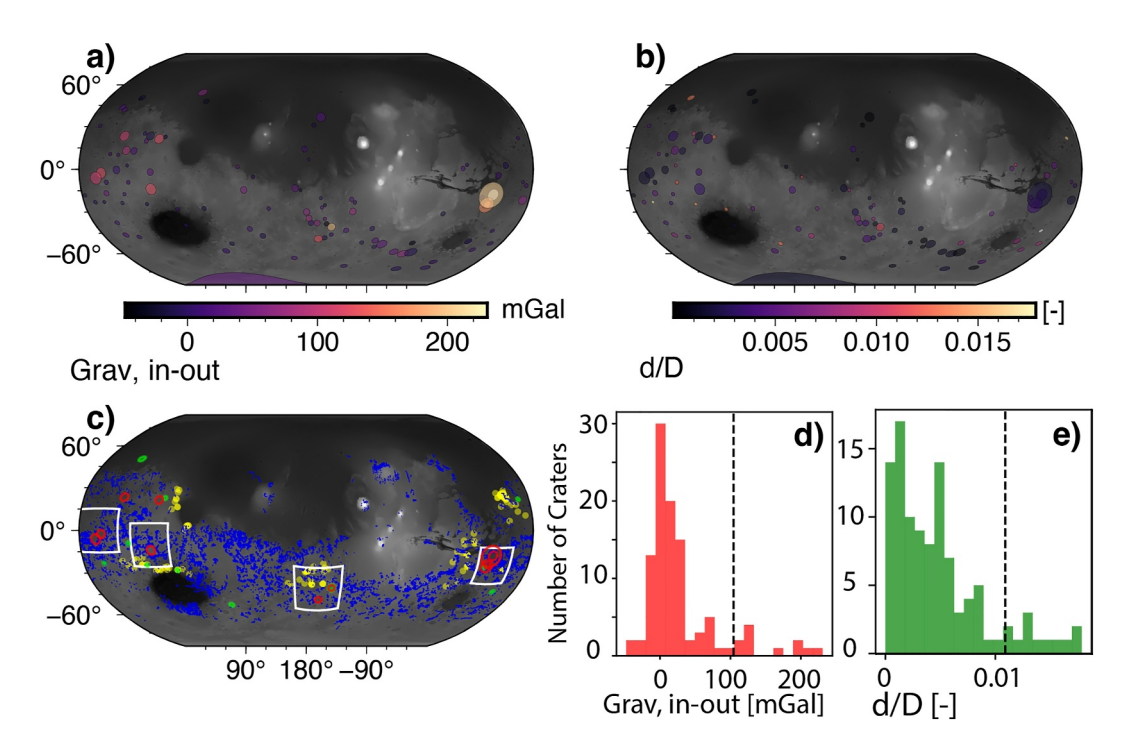


Figure 1. Global analysis of Bouguer gravity signatures associate with craters larger than 150 km (except HUIA) (a) the gravity difference, that is inner minus the outer Bouguer gravity anomaly, (b) depth diameter (d/D) ratios and, (c) only the 90th percentile of these distributions corresponding to the gravity difference (red), and d/D ratios (green). The white boxes highlight regions we focus on later and are shown in Figure 3 where boxes from left to right correspond to panels 3g–3i, 3j–3l, 3a–3c and 3d–3f, respectively. Valley networks as mapped by Hynek et al. (2010) are shown in blue. Ancient clay formation as mapped by Carter et al. (2015) are shown in yellow. The background maps in panels (a)–(c) are shaded MOLA topography maps. Histograms of those distributions and with the 90th percentile marked by the vertical dashed bar are shown in panel (d) gravity and (e) d/D.

inspecting the correspondence between observed and synthetic data to select the final model. Therefore, the inversion result only marginally depend on the value of the assigned uncertainty.

Further data incorporated in the analysis consists of a catalog of mapped weathering sequences (Carter et al., 2015), and valley networks as mapped by Hynek et al. (2010). Those are used to provide further regional context on the area. We also use MOLA topography for plotting and to assess depth-diameter ratios. We analyze the 109 craters with diameter greater than 150 km in the catalog of Robbins and Hynek (2012), and a subset of those craters has been dated (Supp. Table 3 in Robbins et al. (2013)).

3. Method

3.1. Global Analysis

For all 105 craters with diameter greater than 150 km and excluding the large basins Hellas, Utopia, Isidis and Argyre (HUIA), we evaluate the Bouguer gravity and topography profiles transecting the crater every 30° in azimuth and get the median transect from the center of the crater out to 2 radii. We use topography to adjust the crater rim for cases in which the topographic rim of the transect is slightly inconsistent with the diameter listed in Robbins et al. (2013). This is done by evaluating peaks in the median transect and adjusting the position if a prominent rim is within 10% distance of the rim, where 100% corresponds to the crater diameter. We then evaluate the depth diameter ratio (d/D) by selecting the difference between the minimum transect value within $0.2 \times R_{crater}$ and the median transect value between 1 and $1.2 \times R_{crater}$ for the depth divided by the crater diameter. We also assess if the crater is associated with a high Bouguer gravity anomaly by subtracting the median within $0.2 \times R_{crater}$ from the median outside the crater and between 1 and $1.2 \times R_{crater}$ of the transect. We will call this quantity gravity difference for the remainder of the paper. We evaluate the 90th percentile of those values to define the most extreme cases of craters with large d/D ratios and gravity differences (Figure 1). This analysis

MITTELHOLZ ET AL. 5 of 19

allows identifying craters that experienced limited relaxation, which we interpret as proxy for hydrothermal circulation. Based on this analysis, we select regions for more detailed modeling.

3.2. Joint Inversion of Density and Magnetization

Inversions of potential fields are inherently non-unique. However, individual magnetic and gravity inversions sense structures differently and thus have different trade-offs in the model structure. For this reason, a joint inversion of the two data sets can reduce the set of acceptable models and lead to improved results (Bosch et al., 2006; Moorkamp et al., 2016). On Earth, such methods are widely employed for different combinations of geophysical data (e.g., reviewed in Gallardo and Meju (2011), Haber and Holtzman Gazit (2013), and Moorkamp (2017)). A crucial ingredient in joint inversion approaches that involve different physical properties, for example, density and magnetization, is the coupling term that defines the expected relationship between those properties. The impact of the choice of coupling on the inversion results has been discussed previously (Bosch, 2016; Meju & Gallardo, 2016; Moorkamp et al., 2011).

The method of choice in this study employs a variation of information constraint that prefers models in which parameters are related. Correlations of the data sets are expected in cases where the same process has led to the density and magnetization signature. In cases where no such solution exists, it is not possible to fit both observed data sets while simultaneously fulfilling the imposed similarity criterion (Moorkamp, 2022). For gravity and magnetic field data, recent studies have shown how such a joint inversion can significantly improve the results and lead to better interpretations (Lösing et al., 2022; Lowe et al., 2024; Wansing et al., 2024). Thus, our approach allows us to evaluate whether gravity and magnetic signatures are related, in our case due to hydrothermal circulation, and if so, how magnetization and density are affected. A clustering analysis can highlight regions of parameter relations and provide a useful tool for subsequent analysis.

3.2.1. Joint Inversion

We use the inversion framework jif3D (Moorkamp et al., 2011) with a recently developed coupling constraint based on variation of information (Moorkamp, 2021) to jointly invert for magnetization and density structure. Variation of information (VI) was only recently adapted for geophysical inversions (Moorkamp, 2021, 2022) and is a measure of the amount of information that one variable carries about another variable. The joint inversion solves a non-linear optimization problem and the objective function, Φ , consists of data misfit terms for residual gravity, $\Phi_{d,grav}$, and the vector magnetic field components, Φ_{d,B_i} , where i represents the three components x, y, and z in Cartesian coordinates, regularization terms, $\Phi_{reg,grav}$ and Φ_{reg,B_i} , and the coupling terms between density and each of the magnetic field components, $\Phi_{VI,grav-B_i}$. The coupling term represents the added constraint that connects density with the three components of magnetization and will be discussed in the following. The regularization terms aim to minimize the gradients of adjacent cells of resulting density and magnetization models and thus favors models with smooth lateral variations. The objective function reads as,

$$\Phi = \Phi_{d,grav} + \sum_{i=x,y,z} \Phi_{d,B_i} + \lambda_{reg,grav} \Phi_{reg,grav} + \sum_{i=x,y,z} \lambda_{reg,B_i} \Phi_{reg,B_i} + \sum_{i=x,y,z} \lambda_{VI_i} \Phi_{VI,grav-B_i}, \tag{1}$$

where λ are respective weighting terms. The variation of information is quantified by the Shannon entropy (Shannon, 2001) that is equal to

$$H(a) = -\sum_{i}^{M} p(a_i) \log p(a_i);$$
(2)

and the probability density distribution $p(a_i)$ of a variable a in each cell i = 1...M. Information shared by two variables is called mutual information and is described as

$$MI(a,b) = H(a) + H(b) - H(a,b).$$
 (3)

MITTELHOLZ ET AL. 6 of 19

Wiley Online Library on [07/10/2025]. See the Terms

Figure 2. The different steps performed for each region: Step 1 includes the joint inversion of the data solving for model magnetization and density until, after n iterations, an acceptable rms and coupling of the model is reached. The initial high coupling weight of 10^6 is lowered one order of magnitude and down to 10^3 once the inversion plateaus to improve the rms misfit (shown by vertical dashed lines in the rms misfit/coupling plots). These are tracked in the rms misfit and coupling. The final model fits the data, while also preserving parameter relationships, that is, coupling. Step 2 shows the resulting model, a final 3D model of the magnetization components and density. In step 3, a clustering analysis of magnetization amplitude versus density highlights distinct regions in the 3D space that provide the basis for further analysis.

If the variables a and b are completely independent, the mutual information term, MI, is large. If however they are related, MI is small. Finally, this information can be incorporated in the objective function as a variation of information term, VI, which can be minimized to favor results in which parameters are related:

$$VI(a,b) = 2H(a,b) - H(a) - H(b) = H(a) + H(b) - MI(a,b)$$
(4)

Parameters a and b represent the normalized density and magnetization components, that is, the inversion favors model with parameter relationships in density with each magnetization component. An iterative non-linear optimization method based on the limited memory quasi-Newton method (Avdeev & Avdeeva, 2009) is used for the inversion and is described in detail in Moorkamp et al. (2011).

We run the inversion starting with a high degree (10^6) of coupling, that is, large λ_{VI_i} , until the data root mean square misfit does not improve further and reaches a plateau (Step 1 in Figure 2 and misfit plots Figures S2–S5 in Supporting Information S1). This ensures that the inversion initially produces models with a high degree of similarity. If the misfit is not satisfactory at this point, we lower λ_{VI} by one order of magnitude, which results in less coupling and allows for lower misfits. Such a reduction is required because the data cannot be adequately fit with such similar models and thus we have to allow for some degree of discrepancy between density and magnetization structures. We repeat this procedure three times lowering λ_{VI_i} to 10^3 ; this has shown to reach a reasonable data misfit with no substantial improvements even when lowering the coupling term. Regularization

MITTELHOLZ ET AL. 7 of 19



weights for magnetization and density remain constant for all runs. They are low, 10 for magnetization and 100 for density, so that the coupling term dominates. This strategy initially enforces strong coupling, but then releases this constraint allowing for limited parameter relationships if required by the data.

The outcome of the inversion is a 3D model of the three components of magnetization and density variations around the mean within the given area (Step 2 in Figure 2). Because directionality of magnetization is non-unique and we are investigating strength of magnetization only, we focus on the amplitude of the derived 3-component magnetization for the following analysis. The model resolution is 60×60 km with a vertical resolution, that is, crustal layer thickness, of 1 km increasing by a factor of 1.1 with depth. Maximum depth is 40 km for all regions but Eridania, which is in an area of particularly thick crust. There, thickness is set to 72 km. We note, that changing of the thickness layer results in weaker/strong magnetization for a thicker/thinner crust, but does not change the overall relative distribution of magnetization within the crust.

3.2.2. Clustering

To evaluate how density and magnetization are related, we perform a clustering analysis in the density/magnetization space of the final model (Step 3 in Figure 2). We use a k-means clustering algorithm which represents an unsupervised machine learning algorithm used for partitioning a data set into k distinct, non-overlapping clusters (Hartigan & Wong, 1979). It operates by iteratively assigning each data point to the nearest cluster centroid and then recalculating the centroids based on the mean of the data points assigned to each cluster. This process continues until convergence, resulting in clusters that minimize the within-cluster sum of squared distances. The amount of clusters (k) is pre-selected based on visual inspection of the magnetization versus density plot. Note that the main goal is to extract data associated with anomalous craters, and with the chosen clustering, we can achieve this well.

4. Result

4.1. Identifying Unrelaxed Craters

In our global population of large craters, the distribution of observed Bouguer gravity differences (Figure 1a) has a mean of 28 mGal with a standard deviation of 52 mGal. The 90th percentile of the distribution is at 104 mGal with a maximum at 204 mGal at Ladon crater. We similarly evaluate the mean d/D ratio (Figure 1b), and the highest values are in proximity to regions with high Bouguer gravity anomalies. Generally, most craters have low d/D ratios and their interior versus exterior gravity differences is around 0, that is, they do not exhibit Bouguer gravity signatures (Figures 1d and 1e).

While there is a bias of large craters being located in the Southern highlands, we still observe clustering of unrelaxed craters in certain areas. Thus, we next select craters that show Bouguer gravity differences larger than the 90th percentile of the 105 evaluated crater signatures to identify regions of interest (Figures 1c–1e and 3). Note that because the size of the crater affects its gravity signature, we have also taken this into account by dividing the Bouguer gravity anomaly by diameter. This results in the same selection of large anomalies when taking into account the 90th percentile (see Figure S1 in Supporting Information S1). The observation of regional clustering of high d/D and large gravity differences is indicative of a common origin and is consistent with these characteristics resulting from a lack of relaxation due to hydrothermal circulation. Anomalous craters are located in places in which ancient clays and fluvial networks are mapped (Figure 1c), indicators that water rock reactions were at least active on the surface. In addition to the region around Eridania (central box) and Ladon (right box), we select regions around Schiaparelli and Huygens craters (left boxes) for the subsequent analysis. In those model regions, the gravity anomalies associated with individual craters stand out quite clearly (Figures 3b, 3e, 3h, and 3k), whereas their magnetic signature is less pronounced (Figures 3c, 3f, 3i, and 3l).

4.2. Magnetization and Density Models From Joint Inversions

Combined modeling using a variation of information constraint allows driving inversion results toward a solution in which density and magnetization are related if the data allow for it. We can therefore uniquely focus on identifying parametric relationships between those properties. We perform multiple iterations, 636 for Schiaparelli, 623 for Huygens, 530 for Ladon, and 973 for Eridania, to ensure a low misfit in combination with strong coupling (misfit plots for all inversions are shown in the Figures S2–S5 in Supporting Information S1).

MITTELHOLZ ET AL. 8 of 19

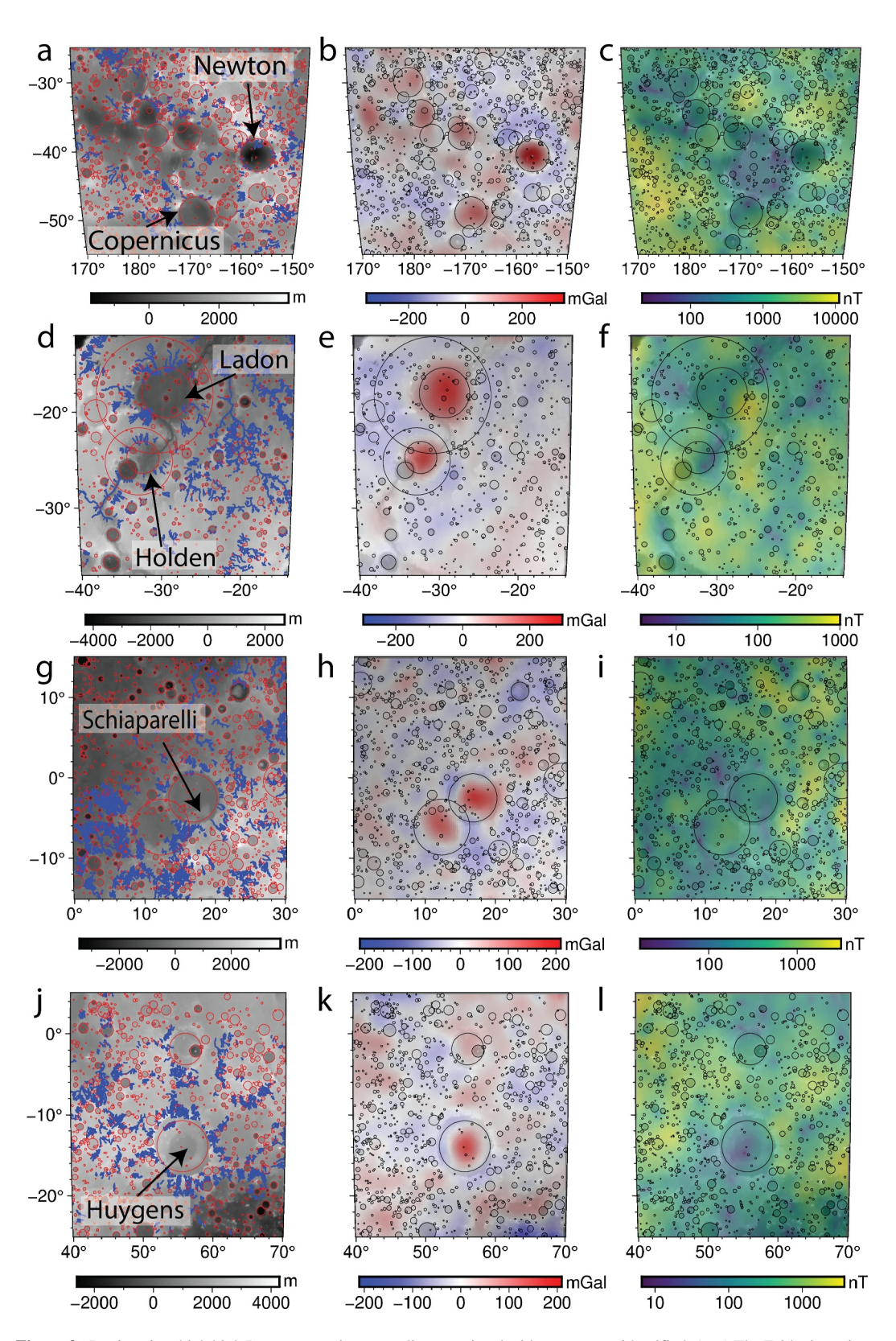


Figure 3. Regions in which high Bouguer gravity anomalies associated with crater were identified: (a–c) The Eridania region with Newton and Copernicus, (d–f) the region around Ladon, (g–i) around the Schiaparelli crater and (j–l) the Huygens crater. The left column shows topography, with valley networks plotted on top (Hynek et al., 2010; blue) and craters highlighted, the second column shows residual gravity and the last column, magnetic field amplitude at 130 km.

MITTELHOLZ ET AL. 9 of 19

21699100, 2025, 4, Downloaded from https://agupubs.onlinelibrary.wiley.com/doi/10.1029/2024JE008832 by Dtsch Zentrum F. Luft-U. Raum Fahrt In D. Helmholtz

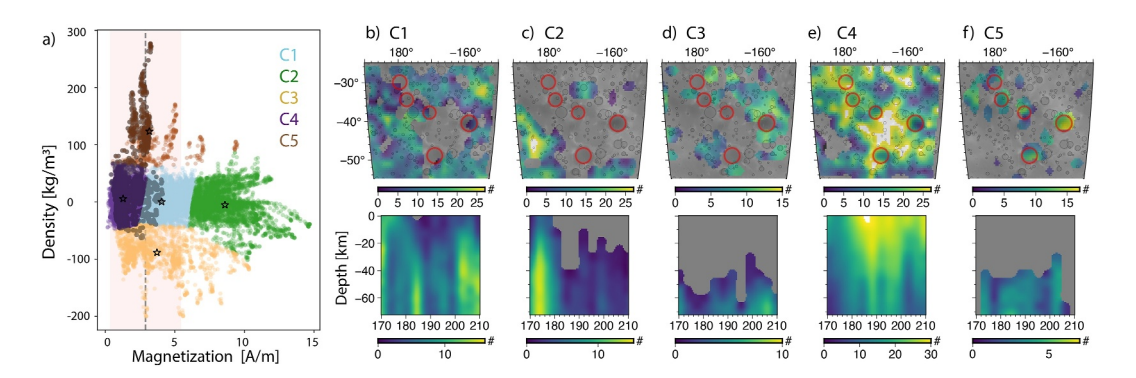


Figure 4. Eridania Cluster—(a) Magnetization versus density and clusters from the ks clustering analysis. Points falling within the red circled craters in later panels are black. The red shaded region indicates the mean ± standard deviation of the regional magnetization. (b)–(f) Color indicates the number of voxel points within clusters C1 to C5 (a) with longitude and (upper) latitude/(lower) depth to showcase the spatial distribution of clusters within the region. The upper row represents a topview and the lower a side-view of the region. Highlighted craters include Newton, Copernicus, and Eridania I, II and III craters (from right to left), that are associated with gravity anomalies.

4.2.1. Eridania

The first region of interest encompasses Eridania, for which hydrothermal alteration has been suggested previously (Ojha et al., 2021). It is situated within some of the strongest magnetic field anomalies on Mars (Mitteholz & Johnson, 2022) and shows morphological evidence for multiple episodes of volcanism (Michalski et al., 2024). A so-called Eridania sea has been hypothesized in the area (Michalski et al., 2017) and shorelines have been suggested between 700 and 1,100 km in MOLA topography.

Our joint inversion and subsequent clustering approach shows several clusters (cluster abbreviated by C) that are mostly driven by density variations (Figure 4a). Dominant high density features associated with craters can easily be identified (C5) and dominantly correspond to magnetization of average and lower than average amplitude within the model region. This cluster is generally found in the lower half of the crust and the corresponding mass surplus is consistent with an uplifted crust-mantle interface, as discussed earlier. For the shown model with a total vertical extent of 75 km, this is deeper than 35 km depth. Note that reducing the total extent of the crust resulted in a similar relative depth distribution (not shown). Most of the upper crust represents material of average density and weakest magnetization (C4). The strongest magnetization (C2) is located at the SW edges of the modeled region and falls outside the topography isolines, representing suggested shorelines of a putative Eridania Sea (Figure 5). Material of similar density, but with weaker magnetization (C1) is broadly distributed and along the shoreline transition. Lowest density material (C3) is also found in the lower crust and seems to be present around regions of high density (C5), that is, around craters. The magnetization of the vertical column above marked craters, but also in general within the region of the proposed Eridania Sea is comparably small (Figure 5).

4.2.2. Huygens

The next region encompasses Huygens crater and south of it Schroeter crater (Figure 6). Similar to the Eridania region, the high residual gravity signature and derived density is very pronounced and up to 300 kg m⁻³ higher than the average density for the overall region (C3). Surrounding material again tends to show lower than average density (C2), with mostly average, but partially large magnetization up to 7 A/m. The magnetization signature in regions of high density however is comparable to the overall region. Strongest magnetization (C5) occurs west of Huygens unrelated to any obvious surface feature and together with C1 it covers magnetizations from 2 to 8 A/m mostly in the mid-crust, but also covering the full vertical extent. Similar to other regions, the upper crust is mostly of average density and minimal magnetization (C4). Similar to the Eridania region, the area stands out in their notable lack of magnetization associated with anomalous craters and surroundings.

4.2.3. Schiaparelli

Schiaparelli and its surroundings are once again similar in the pronounced density signal at depth (Figure 7; C1). The crater associated magnetization is however slightly higher than average especially for regions in the lower

MITTELHOLZ ET AL. 10 of 19

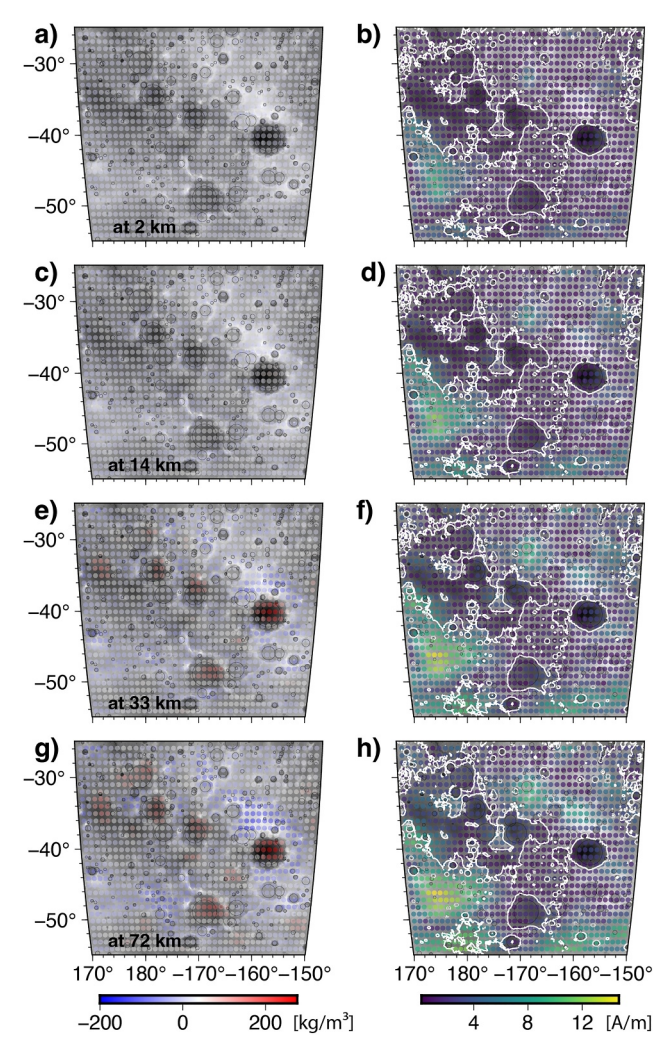


Figure 5. Eridania - Models of (left) density and (right) magnetization at variable depths. Topography lines at 1,100 km indicate proposed shorelines of a standing body of water in the region (Michalski et al., 2017). Corresponding figures for other regions are in the supplement (Figures S6–S8 in Supporting Information S1).

half of the crust. Other more strongly magnetized regions are distributed across the region and are mostly of average density (C2) and in the lower and mid crust. The last cluster (C3) corresponds to average density and near-zero magnetization dominating the upper crust, but also deeper sections.

4.2.4. Ladon and Surroundings

Lastly, the region encompassing Ladon (Figure 8) shows distinct residual gravity anomalies that are linked to two distinct magnetic signatures and magnetization within the cluster is more than a standard deviation higher than the average magnetization (C1). While these anomalies are mostly associated with the deeper crust, they are also visible at shallow depths. One anomaly is localized in the inner region of Ladon, a large multi-ring basin with a total diameter of >1,000 km. The second anomaly is located NE of Holden crater. The anomaly encircles what is listed as crater in the Robbins et al. (2013) database, but was mapped because of its gravity anomaly rather than its topographic expression and might not actually represent a crater. Note that some higher magnetizations are also related to some regions of average and lower than average density (C2). Again, most of the upper crust defines the average density and is associated with very weak magnetization. Generally, average magnetization in this region is lower compared to other investigated locations.

5. Discussion

5.1. Global Distribution of Bouguer Gravity Anomalies

While individual craters or regions have been shown to exhibit peculiar superisostatic gravity anomalies (Mohit & Phillips, 2007; Ojha et al., 2021), Figure 1 shows the global distribution of such signatures.

Previously, Mohit and Phillips (2007) showed that most basins with diameters between 275 and 1,000 km exhibit very shallow depths and limited crustal thinning, indicating that viscoelastic relaxation was a dominant geological process. Consistent with this, our results show that the majority of large craters on Mars display shallow depth and small interior-to-exterior Bouguer gravity anomalies (Figures 1d and 1e), further suggesting that crustal relaxation occurred after most impact events. Only a few craters show a lack of notable viscoelastic relaxation, with Newton, Copernicus, and Ladon being notable exceptions previously identified (Mohit & Phillips, 2007). These, along with others, also stand out in our analysis (center and right box in

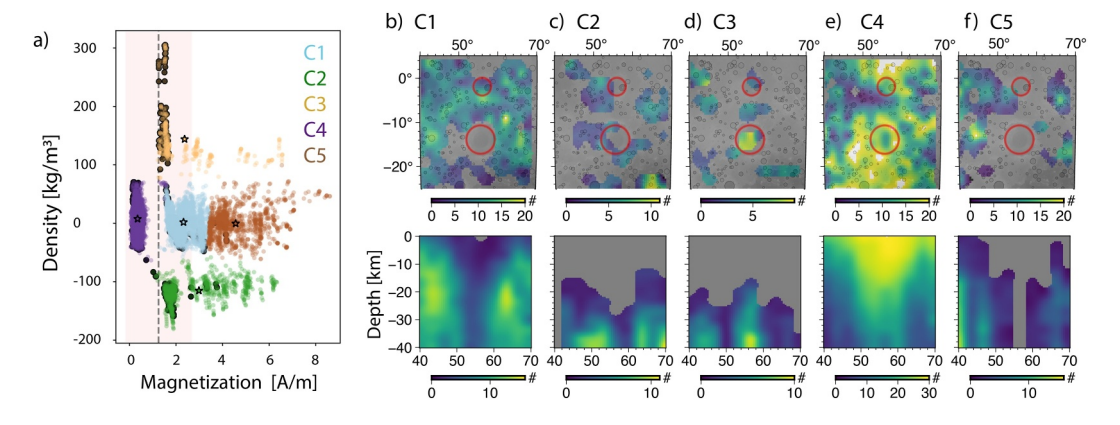


Figure 6. Huygens Cluster—equivalent to Figure 4.

MITTELHOLZ ET AL. 11 of 19

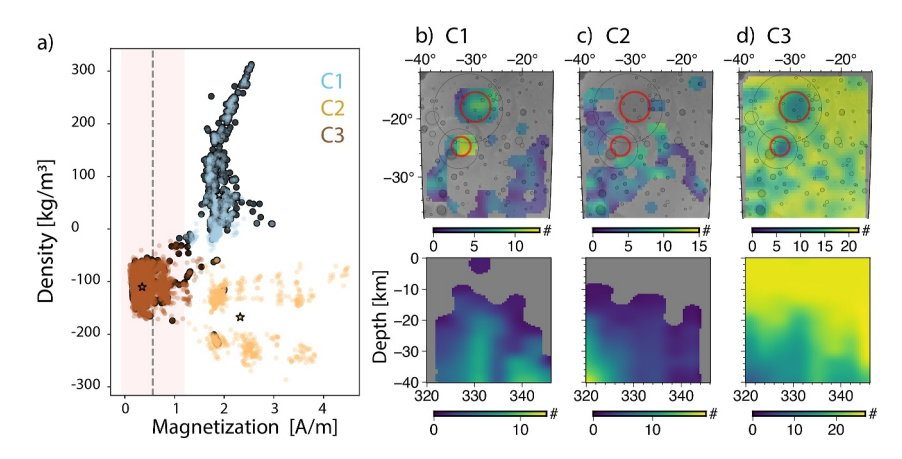


Figure 7. Schiaparelli Cluster—equivalent to Figure 4.

Figure 1). Additionally, a cluster of craters with "anomalous" gravity and topographic signatures is observed south of Arabia Terra, encompassing craters such as Schiaparelli and Huygens (left boxes).

On the Moon, large basins have distinct gravity signatures that are, however, different from Martian ones. This is because the so-called lunar mascons (from mass concentrations), generally form from upward displacement of the crust/mantle interface and infilling from dense mare basalts. In addition to a positive Bouguer anomaly within the inner peak ring followed by a negative Bouguer anomaly of the outer ring up to the crater rim, lunar basins show distinct free-air anomalies (Neumann et al., 2015). This gravitational signature is not observed for most Martian basins (e.g., Mohit & Phillips, 2007; Ojha et al., 2021). On the Moon described gravity anomalies are common, while on Mars, we identify only few craters with large Bouguer anomalies that are distinctly different from the rest of the crater population (Figure 1). As such, a direct comparison with the Moon is not appropriate, and instead the origin of such signatures on Mars points toward more local geological processes.

Rapid cooling of the crust due to hydrothermal circulation following the impact event has been proposed as an explanation for the lack of compensation (Mohit & Phillips, 2007). A subsequent study focusing on the Eridania region including Newton and Copernicus corroborated those findings (Ojha et al., 2021). This study combined geochemical, gravity, and topography data with numerical models, confirming that radiogenically driven hydrothermalism was likely a dominant process in the region. Clays in the vicinity of Eridania (Figure 1c; Carter et al., 2015), but also of the other investigated regions, as well as indications of water run-off in the form of valley networks, point toward water - surface interactions. This is indicative of water present not only in the subsurface but also at the surface.

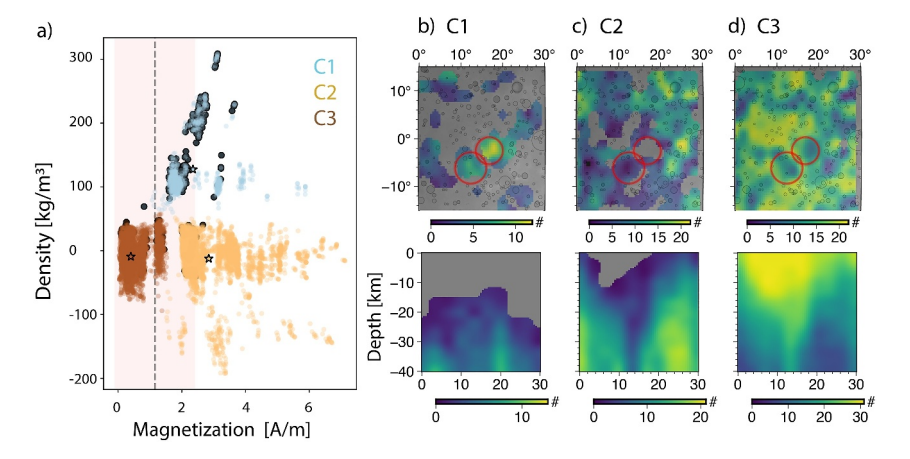


Figure 8. Ladon Cluster—equivalent to Figure 4.

MITTELHOLZ ET AL. 12 of 19

Interestingly, the distribution of anomalous craters follows the equator if one takes into account subsequent true polar wander due to the emplacement of Tharsis as suggested by Bouley et al. (2016). The authors explained the high concentration of valley networks in the paleo-tropical band by Tharsis-driven polar wander, a scenario in which large-scale volcanism was active after the emplacement of the majority of valley networks. This is also later than the latest indications of an active dynamo (Mitteholz & Johnson, 2022) and could be related to increased heat flux, possibly in addition to increased HPEs as drivers for hydrothermal circulation.

5.2. Association With Magnetic Signatures

In general, for all craters selected based on their anomalous gravity signatures, a distinct density signal is observed (Figures 4 and 6–8). In all regions, elevated density originates in the lower half of the crust and deeper, consistent with a lack of relaxation, that is, superisostasy, of the crust—mantle interface. The areas surrounding the craters tend to exhibit lower crustal densities than average, which may be attributed to increased porosity from impact-induced brecciation, highly porous impact ejecta, and/or crustal thickening. In particular, impact-induced brecciation has been the focus of a recent modeling study that showed an increase in porosity within the area around the crater (Wiggins et al., 2022). In addition, Venkatadri and James (2020) showed that 76% of their population of studied lunar craters showed high porosities down to 10s of km in the vicinity of craters, while the interior showed relatively low porosities due to pore-closure from impact melt. These observations are consistent with our models. High porosity from impact-induced brecciation or crustal thickening can generate pathways for water, and thus increased CRM or simply more crustal magnetizable material in the presence of a dynamo.

Magnetic field signatures are not as clearly discernible and the use of the joint inversions allows us to test whether any possible parameter relationships between residual gravity and magnetic fields are permissible by the data. The unclear association of residual gravity anomalies with magnetic signatures is not surprising, because magnetic anomalies are related to the absence or presence of a dynamo field, along with potential post-impact modifications to the magnetic signature that are unrelated to the impact event itself. In general, and not limited to crater signatures, the strongest magnetization is found within the lower crust, consistent with previous estimations of source depth, which indicated deep magnetic sources in the southern hemisphere crust (Gong & Wieczorek, 2021). In contrast, the upper crust is typically weakly magnetized. Additionally, magnetization within the craters is relatively weak and close to the crustal average, which generally corresponds to the least magnetized areas, particularly in regions around Eridania and Huygens. In contrast, Schiaparelli shows elevated magnetization compared to the crustal average, but dissimilar to other regions in the mid and lower crust. For Ladon, magnetization within the crater is notably higher and distinct from surrounding magnetization.

All investigated craters are older than 3.75 billion years (see Figure 9) and were likely formed when a dynamo was active. If impact-related processes, that is, heating and shock, had a significant effect, one might expect either a "demagnetization" signature, which is lower interior magnetization compared to the surroundings, or a "magnetization" signature, where interior magnetization is higher, depending on the dynamo's activity at the time. Similarly, if hydrothermal activity was dominant, CRM in the presence of a dynamo field would have resulted in a magnetization signature. While Ladon shows a potential magnetization signature, no distinct magnetization signature is observed in the other regions. What are possible reasons for a dominant lack of such signatures?

Recent study showed that most craters, not only the ones studied here, do not exhibit distinct magnetization signatures, with demagnetization signatures being far more common (Mittelholz et al., 2024). Excavation, where crustal material with higher susceptibility compared with most mantle mineralogies within craters is removed (Mittelholz et al., 2024), or cooling in a reversing field (Steele et al., 2024), are both plausible explanations for the presence of demagnetization signatures, even in the presence of a dynamo field that should otherwise result in a magnetized crater interior. These effects are particularly important for large craters that excavate major portions of crustal material and cool slowly, but they also heavily depend on local mineralogy, crustal thickness, and reversal timescales. However, such processes should still produce distinct signatures associated with crater topography, rather than affecting the overall region, as observed in the craters studied here.

Despite the inversion process favoring models with distinct crater signatures (i.e., distinct clusters), we observe a mostly non-distinguishable crater magnetization from the immediate crater surroundings, with the exception of Ladon and Schiaparelli. This observation is consistent with long-lasting hydrothermal alteration. If the crust was hydrothermally altered through rock-water interactions at the time of the impact and after, CRM might have been an ongoing process and possibly overprinted any pre-existing magnetization of the crater, but also of the

MITTELHOLZ ET AL. 13 of 19

21699100, 2025, 4, Downloaded from https://agupubs.onlinelibrary.wiley.com/doi/10.1029/2024JE008832 by Disch Zentrum F. Luft-U. Raum Fahrt In D.

Wiley Online Library on [07/10/2025]

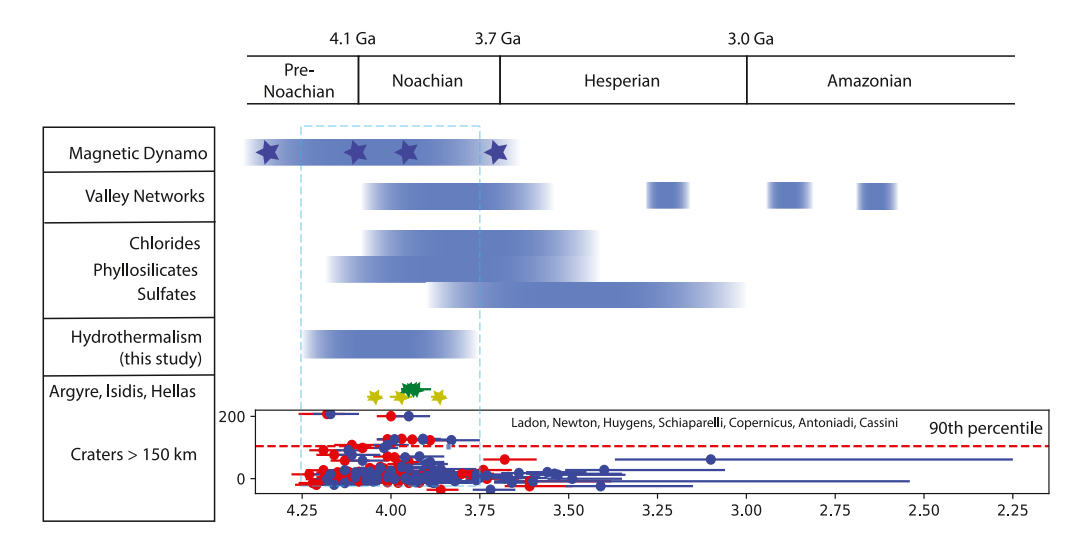


Figure 9. Timing of major events on Mars (modified from Ehlmann & Edwards, 2014). The gradient indicates uncertainty in the data. For the magnetic dynamo, stars indicate specific times for which evidence for a dynamo exist (Mittelholz et al., 2020; Steele et al., 2023) to clarify that weaker or interrupted periods between are theoretically possible. Valley Network timing constraints come from Fassett and Head (2008). The timing of the large basins Hellas, Isidis and Argyre are shown in green (dark is for Hartmann (2005) and light for Neukum et al. (2001) chronology). Other timed basins (a subset of all craters larger than 150 km; Robbins & Hynek, 2012) are shown with their corresponding difference in gravity inside minus outside the crater. The red dashed line highlights the 90th percentile of the distribution. Blue/Red shows ages from Hartmann (2005) and Neukum et al. (2001) chronologies respectively. The blue box highlights the time frame of impacts for the high Bouguer gravity signature craters that provides a timing constraint on hydrothermalism.

surroundings. In absence of a dynamo, this process would remove any magnetization. For Eridania, this scenario is further supported by the absence of magnetic signatures beyond investigated craters within what has been hypothesized to have been the Eridania sea, a region within a topographic low (Michalski et al., 2017). A standing body of water, likely percolating through the crust and pooling in the form of groundwater could have been responsible for demagnetizing the entire Eridania basin compared with its surroundings (Figure 5). Observed lower than average density around the crater anomalies and associated crater induced brecciation could be enhanced by serpentinization reactions because of crustal percolation. Serpentinization has shown to lead to decreased densities (Quesnel et al., 2009); this might be a further indicator that such reactions were occurring within the region and at depth.

If the observed depth distribution of magnetic anomalies in model regions is truly due to hydrothermal circulation, then this could mean that hydrothermal circulation on Mars and associated alteration could have reached substantial depths leading to magnetization or demagnetization within the area, particularly interesting around Eridania, which is located in a region of extremely thick crust but shows a regional demagnetization. Note that the crustal thickness for the Eridania and Huygens regions is thicker than for the other two regions (Wieczorek et al., 2022). While the absolute value of crustal thicknesses varies depending on assumptions on crustal density, crustal thickness around Ladon and Schiaparelli are only approximately 80% of thicknesses around Eridania and Huygens for the suite of models published by Wieczorek et al. (2022). This could support the hypothesis that observed hydrothermalism is strongly coupled to the presence of HPEs of which a larger amount is available in regions of thicker crust (Frizzell et al., 2023). One of the lines of evidence for radiogenically driven hydrothermalism came from the observation of large amounts of HPE in the shallow subsurface of Eridania basin, which was argued to be associated with elevated regional heat flux in the Noachian (Ojha et al., 2020, 2021). How does this compare with the other investigated regions? We adapt the same heat flow model from the previous study (see Text S1 in Supporting Information S1) and evaluate the other regions investigated in this study. High heat flux associated with Eridania clearly stands out (Figures 10c and 10e). Ladon, the only region with a clear magnetization signature is the one with the lowest Noachian heat flux and HPE concentrations (Figure 10), even below the average between -60 and 60° latitude. The region around Schiaparelli shows only slightly increased heat flux compared to the average. Interestingly, the region around Huygens that shows magnetization within the area, even if not clearly associated with the Schiaparelli crater itself is characterized by relatively high heat flux.

MITTELHOLZ ET AL. 14 of 19

21699100, 2025, 4, Downloaded from https://agupubs.onlinelibrary.wiley.com/doi/10.1029/2024JE008832 by Disch Zentrum F. Luft-U. Raum Fahrt In D. Helmholtz Gemein.

Wiley Online Library on [07/10/2025]. See the

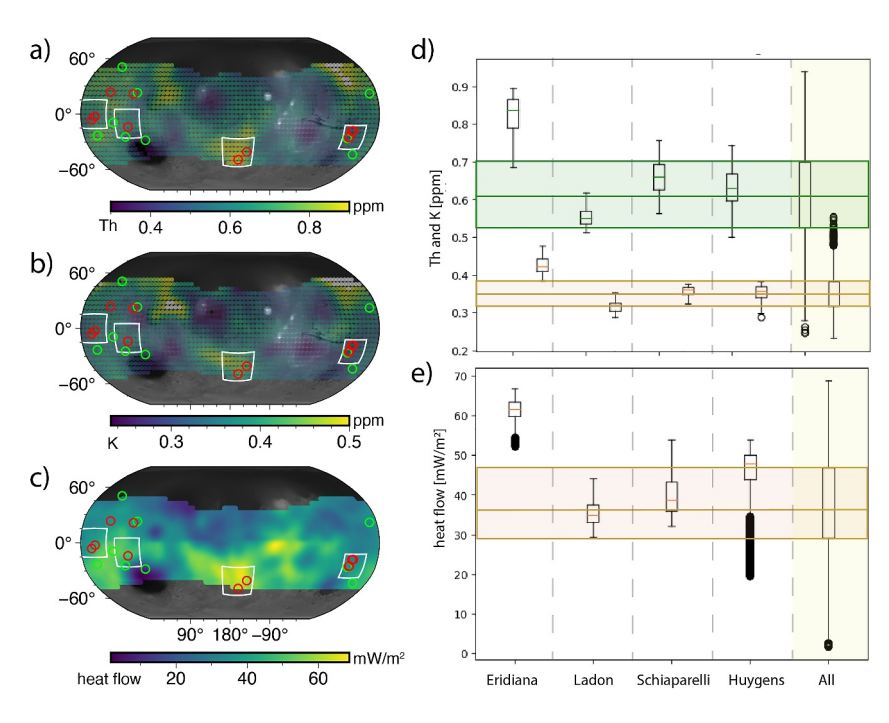


Figure 10. (a) Th and (b) K concentration in the shallow subsurface every 5° in longitude and latitude from the Mars Odyssey Gamma Ray Spectrometer suite. (c) Surface heat flow estimates for Noachian Mars. (a)–(c) Increasing H abundance results in numerical uncertainty for HPE concentrations in the polar latitudes and such areas are excluded. (d) Th (green) and K (orange) box diagrams representing areas within outlined boxes around Schiaparelli, Huygens, Eridania and Ladon (from left to right) compared with the (unmasked) global average. Box car plots show the median (orange) in a box ranging from the first to the third quartile. Minimum and maximum, and outliers (black circles) are shown. (e) Equivalent to (d) but for heat flow.

The significant enrichment of thorium and potassium has been interpreted as evidence that hydrothermalism in the Eridania region was powered by radiogenic heat (Ojha et al., 2021) with these concentrations following a trend of greater enrichment in areas with weaker magnetization compared to their surroundings. A recent study by Frizzell et al. (2023) also showed that the shallow subsurface concentrations of heat-producing elements (HPE) such as Th, K and U, as measured by the Mars Odyssey Gamma Ray Spectrometer Suite (GRS; Boynton et al., 2007), must increase with crustal depth to align with seismic data from the InSight mission. Additionally, they found that variations in crustal heat flow are most significantly influenced by changes in crustal thickness. In conclusion, the observed trend of high heat flux and elevated Th and K concentrations in areas of reduced magnetization supports the interpretation that increased crustal thickness enhances the availability of HPEs. This reinforces the idea that radiogenic heating driving hydrothermal activity in the crust may modulate the degree of magnetization signatures observed on Mars.

The percolation of liquid water to significant depths may be facilitated by rock fracturing caused by impact events, which creates pathways for water circulation. The increased availability of HPE could then sustain long-term hydrothermal systems over geological timescales. This process could potentially lead to demagnetization down to the crustal base, as observed in the Eridania and Huygens regions. Alternatively, the high heat flux in some areas may have raised crustal temperatures above the Curie temperature of certain magnetic minerals (Dunlop & Arkani-Hamed, 2005), particularly at greater depths, allowing for magnetization or demagnetization processes to occur. This could either mean that magnetization observed in potentially hydrothermally affected regions, such as around Ladon or Schiaparelli, may result from a dynamo that persisted longer than the hydrothermal system due to limited HPE availability and regional crustal cooling. Alternatively, the limited depth of percolation could have demagnetized only the upper and mid crust, while the deeper demagnetization observed in Eridania and Schiaparelli may be attributed to thermal effects occurring after dynamo cessation, possibly facilitated by a higher concentration of HPEs. Either way, these observations constrain the timing of hydrothermal activity to periods after the dynamo ceased to operate. The most recent evidence for an active dynamo comes from the crustal field signature at Lucus Planum in the Medusae Fossae Formation, dated to 3.7 Ga (Mittelholz

MITTELHOLZ ET AL. 15 of 19

et al., 2020; Ojha & Mittelholz, 2023). The absence of magnetic anomalies in the region of a plume in Elysium Planitia suggests that the dynamo shut down before volcanism ceased in this region, approximately 3.5 Ga (Broquet & Andrews-Hanna, 2023). If hydrothermal circulation is indeed responsible for demagnetizing large portions of the crust, it must have been active past 3.7 Ga and possibly persisted for longer periods throughout large portions of the crust. This is a notable finding, as hydrothermal systems are considered key environments for sustaining conditions conducive to early life on Mars.

Lastly, Ladon stands out in terms of magnetization due to the distinct magnetization signature within the basin, as previously noted by Lillis et al. (2013). Ladon is the oldest and largest of all the investigated craters. Geographically it is at the eastern edge of Valles Marineris and hydrothermal activity on Mars and associated magnetic signatures have previously been suggested at this location (Gurgurewicz et al., 2022). Hydrothermal activity in this area was dated to Pre-Noachian and it is feasible that this activity ceased earlier compared to the other regions, allowing for the crater to record a magnetization signature. As mentioned, a contributing factor could be related to the thinner crust right at the dichotomy with less heat producing elements, thus a shorter period of hydrothermal activity.

We briefly address the magnetic field signatures of a crater in hydrothermal settings on Earth, specifically the Chicxulub crater; this can give some further insight on magnetization signatures due to additional data sets such as cores and higher resolution geophysical data. The 180 km Chicxulub peak-ring crater displays a small central positive gravity anomaly, attributed to Moho uplift beneath the impact site (Gulick et al., 2013), surrounded by a negative anomaly ring corresponding to the peak ring location. Note, however, that the gravity anomaly is small and this region would not have stood out as anomalous (Figure 1). Long-wavelength magnetic anomalies at Chicxulub are explained by strongly magnetized sources in the uplifted lower crust (Ortiz-Alemán & Urrutia-Fucugauchi, 2010; Pilkington & Hildebrand, 2000). These magnetic features are thought to be pre-impact in origin, but recent studies (e.g., Kring et al., 2020) suggest that post-impact hydrothermal systems played a significant role in modifying the crust down to 5–6 km over several million years, further altering the magnetic and structural properties of the impact zone. Paleomagnetic data even indicate that the system persisted for more than 2 million years, spanning a geomagnetic polarity reversal. Of course in case of the Earth, this happened in the presence of a dynamo field. Deep magnetized sources and signs of a hydrothermal system are mostly comparable with the case of Ladon; this is consistent with the hypothesis that hydrothermal circulation and dynamo timing might have been largely happening at the same time in that region.

Finally, local investigations are currently limited by available data sets. For gravity data, a dedicated gravity mission like GRAIL on the Moon or GRACE on Earth would enable a highly improved data set and should be on the list for most wanted missions to Mars (e.g., Genova, 2020; Wörner et al., 2023). While the magnetic field has excellent coverage from orbit, regional studies would allow investigation of features with wavelengths smaller than 100s of km (Mittelholz et al., 2023). Such data sets would enable a more detailed understanding of the 3D crustal structure on Mars. The importance of hydrothermal systems due to their possible association with life on Mars would make any of the investigated regions particularly interesting areas for such missions.

Data Availability Statement

The joint inversion framework jif3D is available under a GNU General Public License (Moorkamp, 2024). All input models are available online (Genova et al., 2016; Langlais et al., 2019) and are also part of the SHTools package (Wieczorek, 2019). The residual gravity data was generated using the DPS package of Broquet (2024). We thank the developers of PyGMT (Uieda et al., 2021) that was used for all map plots in this study.

Acknowledgments

AM acknowledges funding through the SNF Ambizione fellowship, Grant PZ00P2 209123.

References

Acuña, M. H., Connerney, J. E. P., Ness, N. F., Lin, R. P., Mitchell, D., Carlson, C. W., et al. (1999). Global distribution of crustal magnetization discovered by the Mars global surveyor MAG/ER experiment. *Science*, 284(5415), 790–793. https://doi.org/10.1126/science.284.5415.790 Amador, E. S., Bandfield, J. L., & Thomas, N. H. (2018). A search for minerals associated with serpentinization across Mars using CRISM spectral data. *Icarus*, 311, 113–134. https://doi.org/10.1016/j.icarus.2018.03.021

Andreani, M., Muñoz, M., Marcaillou, C., & Delacour, A. (2013). µXANES study of iron redox state in serpentine during oceanic serpentinization. *Lithos*, 178, 70–83. https://doi.org/10.1016/j.lithos.2013.04.008

Avdeev, D., & Avdeeva, A. (2009). 3D magnetotelluric inversion using a limited-memory quasi-Newton optimization. *Geophysics*, 74(3), F45–F57. https://doi.org/10.1190/1.3114023

Blakely, R. J. (1996). Potential theory in gravity and magnetic applications. Cambridge University Press.

MITTELHOLZ ET AL. 16 of 19

- Bonnemains, D., Carlut, J., Escartín, J., Mével, C., Andreani, M., & Debret, B. (2016). Magnetic signatures of serpentinization at ophiolite complexes. *Geochemistry, Geophysics, Geosystems*, 17(8), 2969–2986. https://doi.org/10.1002/2016GC006321
- Bosch, M. (2016). Inference networks in Earth models with multiple components and data. In *Integrated imaging of the earth* (pp. 29–47). American Geophysical Union (AGU). https://doi.org/10.1002/9781118929063.ch3
- Bosch, M., Meza, R., Jiménez, R., & Hönig, A. (2006). Joint gravity and magnetic inversion in 3D using Monte Carlo methods. *Geophysics*, 71(4), G153–G156. https://doi.org/10.1190/1.2209952
- Bouley, S., Baratoux, D., Matsuyama, I., Forget, F., Séjourné, A., Turbet, M., & Costard, F. (2016). Late Tharsis formation and implications for early Mars. *Nature*, 531(7594), 344–347. https://doi.org/10.1038/nature17171
- Boynton, W. V., Taylor, G. J., Evans, L. G., Reedy, R. C., Starr, R., Janes, D. M., et al. (2007). Concentration of H, Si, Cl, K, Fe, and Th in the low-and mid-latitude regions of Mars. *Journal of Geophysical Research*, 112(E12), E12S99. https://doi.org/10.1029/2007JE002887
- Broquet, A. (2024). AB-Ares/Displacement_strain_planet: Version 0.5.0. Zenodo. https://doi.org/10.5281/zenodo.10552129
- Broquet, A., & Andrews-Hanna, J. C. (2023). Geophysical evidence for an active mantle plume underneath Elysium Planitia on Mars. *Nature Astronomy*, 7(2), 160–169. https://doi.org/10.1038/s41550-022-01836-3
- Bultel, B., Wieczorek, M., Mittelholz, A., Johnson, C. L., Gattacceca, J., Fortier, V., & Langlais, B. (2025). Aqueous alteration as an origin of martian magnetization. *Journal of Geophysical Research: Planets*, 130(1), e2023JE008111. https://doi.org/10.1029/2023JE008111
- Carter, J., Loizeau, D., Mangold, N., Poulet, F., & Bibring, J.-P. (2015). Widespread surface weathering on early Mars: A case for a warmer and
- wetter climate. *Icarus*, 248, 373–382. https://doi.org/10.1016/j.icarus.2014.11.011

 Carter, J., Poulet, F., Bibring, J.-P., Mangold, N., & Murchie, S. (2013). Hydrous minerals on Mars as seen by the CRISM and OMEGA imaging spectrometers: Updated global view. *Journal of Geophysical Research: Planets*, 118(4), 831–858. https://doi.org/10.1029/2012JE004145
- Chassefière, E., Langlais, B., Quesnel, Y., & Leblanc, F. (2013). The fate of early Mars' lost water: The role of serpentinization. *Journal of Geophysical Research: Planets*, 118(5), 1123–1134. https://doi.org/10.1002/jgre.20089
- Chassefière, E., Leblanc, F., & Langlais, B. (2007). The combined effects of escape and magnetic field histories at Mars. *Planetary and Space Science*, 55(3), 343–357. https://doi.org/10.1016/j.pss.2006.02.003
- Science, 55(3), 343–357. https://doi.org/10.1016/j.pss.2006.02.003
 Clifford, S. M. (1993). A model for the hydrologic and climatic behavior of water on Mars. *Journal of Geophysical Research*, 98(E6), 10973–
- 11016. https://doi.org/10.1029/93JE00225
 Draeger, U., Prévot, M., Poidras, T., & Riisager, J. (2006). Single-domain chemical, thermochemical and thermal remanences in a basaltic rock.
- Geophysical Journal International, 166(1), 12–32. https://doi.org/10.1111/j.1365-246X.2006.02862.x

 Dunlop, D. J., & Arkani-Hamed, J. (2005). Magnetic minerals in the Martian crust. Journal of Geophysical Research, 110(12), 1–11. https://doi.org/10.1029/2005JE002404
- Dunlop, D. J., & Özdemir, Ö. (2001). Rock magnetism: Fundamentals and frontiers (No. 3). Cambridge University Press.
- Edwards, C. S., Christensen, P. R., & Hamilton, V. E. (2008). Evidence for extensive olivine-rich basalt bedrock outcrops in Ganges and Eos Chasmas, Mars. *Journal of Geophysical Research*, 113(E11), E11003. https://doi.org/10.1029/2008JE003091
- Ehlmann, B. L., & Edwards, C. S. (2014). Mineralogy of the Martian surface. *Annual Review of Earth and Planetary Sciences*, 42(1), 291–315. https://doi.org/10.1146/annurev-earth-060313-055024
- Ehlmann, B. L., Mustard, J. F., Murchie, S. L., Bibring, J.-P., Meunier, A., Fraeman, A. a., & Langevin, Y. (2011). Subsurface water and clay mineral formation during the early history of Mars. *Nature*, 479(7371), 53–60. https://doi.org/10.1038/nature10582
- Fassett, C. I., & Head, J. W. (2008). The timing of martian valley network activity: Constraints from buffered crater counting. *Icarus*, 195(1), 61–89. https://doi.org/10.1016/j.icarus.2007.12.009
- Frizzell, K. R., Ojha, L., & Karunatillake, S. (2023). Bounding the unknowns of Martian crustal heat flow from a synthesis of regional geochemistry and InSight mission data. *Icarus*, 405, 115700. https://doi.org/10.1016/j.icarus.2023.115700
- Gallardo, L. A., & Meju, M. A. (2011). Structure-coupled multiphysics imaging in geophysical sciences. Reviews of Geophysics, 49(1), RG1003. https://doi.org/10.1029/2010RG000330
- Genova, A. (2020). ORACLE: A mission concept to study Mars' climate, surface and interior. *Acta Astronautica*, 166, 317–329. https://doi.org/10.1016/j.actaastro.2019.10.006
- Genova, A., Goossens, S., Lemoine, F. G., Mazarico, E., Neumann, G. A., Smith, D. E., & Zuber, M. T. (2016). Seasonal and static gravity field of Mars from MGS, Mars Odyssey and MRO radio science. *Icarus*, 272, 228–245. https://doi.org/10.1016/j.icarus.2016.02.050
- Gong, S., & Wieczorek, M. (2021). Depth of martian magnetization from localized power spectrum analysis. *Journal of Geophysical Research: Planets*, 126(8), e2020JE006690. https://doi.org/10.1029/2020JE006690
- Goudge, T. A., Morgan, A. M., Stucky de Quay, G., & Fassett, C. I. (2021). The importance of lake breach floods for valley incision on early Mars. Nature, 597(7878), 645–649. https://doi.org/10.1038/s41586-021-03860-1
- Grau Galofre, A., Jellinek, A. M., & Osinski, G. R. (2020). Valley formation on early Mars by subglacial and fluvial erosion. *Nature Geoscience*, 13(10), 663–668. https://doi.org/10.1038/s41561-020-0618-x
- Gulick, S. P., Christeson, G. L., Barton, P. J., Grieve, R. A., Morgan, J. V., & Urrutia-Fucugauchi, J. (2013). Geophysical characterization of the Chicxulub impact crater. Reviews of Geophysics, 51(1), 31–52. https://doi.org/10.1002/rog.20007
- Gurgurewicz, J., Mège, D., Schmidt, F., Douté, S., & Langlais, B. (2022). Megashears and hydrothermalism at the Martian crustal dichotomy in Valles Marineris. *Communications Earth & Environment*, 3(1), 282. https://doi.org/10.1038/s43247-022-00612-5
- Haber, E., & Holtzman Gazit, M. (2013). Model fusion and joint inversion. Surveys in Geophysics, 34(5), 675–695. https://doi.org/10.1007/s10712-013-9232-4
- Hamilton, V. E., & Christensen, P. R. (2005). Evidence for extensive, olivine-rich bedrock on Mars. *Geology*, 33(6), 433–436. https://doi.org/10.1130/G21258.1
- Hanna, J. C., & Phillips, R. J. (2005). Hydrological modeling of the Martian crust with application to the pressurization of aquifers. *Journal of Geophysical Research*, 110(E1), E01004. https://doi.org/10.1029/2004JE002330
- Harrison, K. H., & Grimm, R. E. (2002). Controls on Martian hydrothermal systems: Application to valley network and magnetic anomaly formation. *Journal of Geophysical Research*, 107(E5), 5025. https://doi.org/10.1029/2001JE001616
- Hartigan, J. A., & Wong, M. A. (1979). Algorithm AS 136: A K-means clustering algorithm. *Journal of the Royal Statistical Society. Series C (Applied Statistics)*, 28(1), 100–108. https://doi.org/10.2307/2346830
- Hartmann, W. K. (2005). Martian cratering 8: Isochron refinement and the chronology of Mars. *Icarus*, 174(2), 294–320. https://doi.org/10.1016/j.icarus.2004.11.023
- He, X.-F., Santosh, M., Tsunogae, T., Malaviarachchi, S. P. K., & Dharmapriya, P. L. (2016). Neoproterozoic arc accretion along the "eastern suture" in Sri Lanka during Gondwana assembly. *Precambrian Research*, 279, 57–80. https://doi.org/10.1016/j.precamres.2016.04.006
- Hynek, B. M., Beach, M., & Hoke, M. R. T. (2010). Updated global map of Martian valley networks and implications for climate and hydrologic processes. *Journal of Geophysical Research*, 115(E9), 1–14. https://doi.org/10.1029/2009JE003548

MITTELHOLZ ET AL. 17 of 19

- Jakosky, B. M. (2025). Results from the inSight Mars mission do not require a water-saturated mid crust. Proceedings of the National Academy of Sciences, 122(11), e2418978122. https://doi.org/10.1073/pnas.2418978122
- Jakosky, B. M., Lin, R. P., Grebowsky, J. M., Luhmann, J. G., Mitchell, D. F., Beutelschies, G., et al. (2015). The Mars Atmosphere and Volatile Evolution (MAVEN) mission. Space Science Reviews, 195(1-4), 3-48. https://doi.org/10.1007/s11214-015-0139-x
- Jansen, J. C., Andrews-Hanna, J. C., Li, Y., Lucey, P. G., Taylor, G. J., Goossens, S., et al. (2017). Small-scale density variations in the lunar crust revealed by GRAIL. *Icarus*, 291, 107–123. https://doi.org/10.1016/j.icarus.2017.03.017
- Keszthelyi, L. P., Denlinger, R. P., O'Connell, D. R. H., & Burr, D. M. (2007). Initial insights from 2.5D hydraulic modeling of floods in Athabasca Valles, Mars. *Geophysical Research Letters*, 34(21), L21206. https://doi.org/10.1029/2007GL031776
- Kring, D. A., Tikoo, S. M., Schmieder, M., Riller, U., Rebolledo-Vieyra, M., Simpson, S. L., et al. (2020). Probing the hydrothermal system of the chicxulub impact crater. *Science Advances*, 6(22), 1–9. https://doi.org/10.1126/sciadv.aaz3053
- Langlais, B., Thébault, E., Houliez, A., Purucker, M. E., & Lillis, R. J. (2019). A new model of the crustal magnetic field of Mars using MGS and MAVEN. *Journal of Geophysical Research: Planets*, 124(6), 1542–1569. https://doi.org/10.1029/2018JE005854
- Lillis, R. J., Robbins, S., Manga, M., Halekas, J. S., & Frey, H. V. (2013). Time history of the Martian dynamo from crater magnetic field analysis. Journal of Geophysical Research Educational Planning, 118(7), 1488–1511. https://doi.org/10.1002/jgre.20105
- Lognonné, P., Banerdt, W., Pike, W. T., Giardini, D., Christensen, U., Garcia, R. F., et al. (2020). Constraints on the shallow elastic and anelastic structure of Mars from InSight seismic data. *Nature Geoscience*. https://doi.org/10.1038/s41561-020-0536-y
- Lösing, M., Moorkamp, M., & Ebbing, J. (2022). Joint inversion based on variation of information—A crustal model of Wilkes Land, East Antarctica. *Geophysical Journal International*, 232(1), 162–175. https://doi.org/10.1093/gji/ggac334
- Lowe, M., Jordan, T., Moorkamp, M., Ebbing, J., Green, C., Lösing, M., et al. (2024). The 3D crustal structure of the Wilkes subglacial Basin, East Antarctica, using variation of information joint inversion of gravity and magnetic data. *Journal of Geophysical Research: Solid Earth*, 129(10), e2023JB027794. https://doi.org/10.1029/2023JB027794
- Meju, M. A., & Gallardo, L. A. (2016). Structural coupling approaches in integrated geophysical imaging. In *Integrated imaging of the earth* (pp. 49–67). American Geophysical Union (AGU). https://doi.org/10.1002/9781118929063.ch4
- Mével, C. (2003). Serpentinisation des péridotites abysales aux dorsales océaniques. Comptes Rendus Geoscience, 335(10–11), 825–852. https://doi.org/10.1016/j.crte.2003.08.006
- Michalski, J. R., Deanne Rogers, A., Edwards, C. S., Cowart, A., & Xiao, L. (2024). Diverse volcanism and crustal recycling on early Mars. Nature Astronomy, 8(4), 456–462. https://doi.org/10.1038/s41550-023-02191-7
- Michalski, J. R., Dobrea, E. Z. N., Niles, P. B., & Cuadros, J. (2017). Ancient hydrothermal seafloor deposits in Eridania basin on Mars. Nature Communications, 8(1), 15978. https://doi.org/10.1038/ncomms15978
- Miller, R. C., Grima, C., Gulick, S. P. S., Goudge, T. A., Russell, A. T., Perry, M. R., et al. (2024). Dynamic development of the Athabasca Valles outflow system from volcanic facies and 15 m scale roughness. *Icarus*, 419, 115691. https://doi.org/10.1016/j.icarus.2023.115691
- Mitteholz, A., & Johnson, C. L. (2022). The martian crustal magnetic field. Frontiers in Astronomy and Space Sciences, 9, 895362. https://doi.org/10.3389/fspas.2022.895362
- Mittelholz, A., Heagy, L., Johnson, C. L., Bapst, J., Espley, J., Fraeman, A. A., et al. (2023). Exploring martian magnetic fields with a Helicopter. The Planetary Science Journal, 4(8), 155. https://doi.org/10.3847/psj/ace9c1
- Mittelholz, A., Johnson, C. L., Feinberg, J. M., Langlais, B., & Phillips, R. J. (2020). Timing of the martian dynamo: New constraints for a core field 4. 5 and 3. 7 Ga ago. *Science Advances*, 18(May), 1–8. https://doi.org/10.1126/sciadv.aba0513
- Mittelholz, A., Johnson, C. L., & Morschhauser, A. (2018). A new magnetic field activity proxy for Mars from MAVEN data. Geophysical Research Letters, 45(12), 5899–5907. https://doi.org/10.1029/2018GL078425
- Mittelholz, A., Steele, S. C., Fu, R. R., Johnson, C. L., Lillis, R. J., & Stucky de Quay, G. (2024). Magnetic field signatures of craters on Mars. Geophysical Research Letters, 51(6), e2023GL106788. https://doi.org/10.1029/2023g1106788
- Mohit, P. S., & Phillips, R. P. (2007). Viscous relaxation on early Mars: A study of ancient impact basins. *Geophysical Research Letters*, 34(L21204), https://doi.org/10.1029/2007g1031252
- Moorkamp, M. (2017). Integrating electromagnetic data with other geophysical observations for enhanced imaging of the Earth: A tutorial and review. Surveys in Geophysics, 38(5), 935–962. https://doi.org/10.1007/s10712-017-9413-7
- Moorkamp, M. (2021). Joint inversion of gravity and magnetotelluric data from the Ernest-Henry IOCG deposit with a variation of information constraint. In First international meeting for applied geoscience & energy expanded abstracts (pp. 1711–1715). https://doi.org/10.1190/segam2021-3582000.1
- Moorkamp, M. (2022). Deciphering the state of the lower crust and upper mantle with multi-physics inversion. *Geophysical Research Letters*, 49(9), https://doi.org/10.1029/2021GL096336
- Moorkamp, M. (2024). jif3D. Retrieved from https://svn.code.sf.net/p/jif3d/jif3dsvn/trunk/jif3D
- Moorkamp, M., Heincke, B., Jegen, M., Roberts, A. W., & Hobbs, R. W. (2011). A framework for 3-D joint inversion of MT, gravity and seismic refraction data. *Geophysical Journal International*, 184(1), 477–493. https://doi.org/10.1111/j.1365-246X.2010.04856.x
- Moorkamp, M., Lelièvre, P. G., Linde, N., & Khan, A. (2016). Integrated imaging of the earth: Theory and applications (Vol. 218). John Wiley & Sons
- Morschhauser, A., Lesur, V., & Grott, M. (2014). A spherical harmonic model of the lithospheric magnetic field of Mars. *Journal of Geophysical Research: Planets*, 119(6), 1162–1188. https://doi.org/10.1002/2013JE004555
- Neukum, G., Ivanov, B. A., & Hartmann, W. K. (2001). Cratering records in the inner solar system in relation to the lunar reference system. In R. Kallenbach, J. Geiss, & W. K. Hartmann (Eds.), *Chronology and evolution of mars* (pp. 55–86). Springer.
- Neumann, G. A., Zuber, M. T., Wieczorek, M. A., Head, J. W., Baker, D. M. H., Solomon, S. C., et al. (2015). Lunar impact basins revealed by gravity recovery and interior laboratory measurements. *Science Advances*, 1(9), e1500852. https://doi.org/10.1126/sciadv.1500852
- Ody, A., Poulet, F., Bibring, J.-P., Loizeau, D., Carter, J., Gondet, B., & Langevin, Y. (2013). Global investigation of olivine on Mars: Insights into crust and mantle compositions. *Journal of Geophysical Research: Planets*, 118(2), 234–262. https://doi.org/10.1029/2012JE004149
- Ojha, L., Buffo, J., Karunatillake, S., & Siegler, M. (2020). Groundwater production from geothermal heating on early Mars and implication for early Martian habitability. Science Advances, 6(49), eabb1669. https://doi.org/10.1126/sciadv.abb1669
- Ojha, L., Karunatillake, S., Karimi, S., & Buffo, J. (2021). Amagmatic hydrothermal systems on Mars from radiogenic heat. *Nature Communications*, 12(1), 1754. https://doi.org/10.1038/s41467-021-21762-8
- Ojha, L., & Mittelholz, A. (2023). Insight into the formation mechanism of the Medusae fossae formation on Mars from magnetic field data. *Icarus*, 395, 115471. https://doi.org/10.1016/j.icarus.2023.115471
- Ortiz-Alemán, C., & Urrutia-Fucugauchi, J. (2010). Aeromagnetic anomaly modeling of central zone structure and magnetic sources in the Chicxulub crater. *Physics of the Earth and Planetary Interiors*, 179(3–4), 127–138. https://doi.org/10.1016/j.pepi.2010.01.007

MITTELHOLZ ET AL. 18 of 19



Journal of Geophysical Research: Planets

- 10.1029/2024JE008832
- Osinski, G. R., Tornabene, L. L., Banerjee, N. R., Cockell, C. S., Flemming, R., Izawa, M. R. M., et al. (2013). Impact-generated hydrothermal systems on Earth and Mars. *Icarus*, 224(2), 347–363. https://doi.org/10.1016/j.icarus.2012.08.030
- Parmentier, E. M., & Zuber, M. T. (2007). Early evolution of Mars with mantle compositional stratification or hydrothermal crustal cooling. *Journal of Geophysical Research*, 112(E2), E02007. https://doi.org/10.1029/2005JE002626
- Pilkington, M., & Hildebrand, A. R. (2000). Three-dimensional magnetic imaging of the Chicxulub Crater. *Journal of Geophysical Research*, 105(B10), 23479–23491. https://doi.org/10.1029/2000JB900222
- Plesa, A. C., Grott, M., Tosi, N., Breuer, D., Spohn, T., & Wieczorek, M. A. (2016). How large are present-day heat flux variations across the surface of Mars? *Journal of Geophysical Research: Planets*, 121(12), 2386–2403. https://doi.org/10.1002/2016JE005126
- Quesnel, Y., Sotin, C., Langlais, B., Costin, S., Mandea, M., Gottschalk, M., & Dyment, J. (2009). Serpentinization of the martian crust during Noachian. Earth and Planetary Science Letters, 277(1–2), 184–193. https://doi.org/10.1016/j.epsl.2008.10.012
- Ramstad, R., & Barabash, S. (2021). Do intrinsic magnetic fields protect planetary atmospheres from stellar winds? Space Science Reviews, 217(2), 36. https://doi.org/10.1007/s11214-021-00791-1
- Robbins, S. J., & Hynek, B. M. (2012). A new global database of Mars impact craters larger than 1 km: 2. Global crater properties and regional variations of the simple-to-complex transition diameter. *Journal of Geophysical Research*, 117(6), 1–21. https://doi.org/10.1029/2011JE003067
- Robbins, S. J., Hynek, B. M., Lillis, R. J., & Bottke, W. F. (2013). Large impact crater histories of Mars: The effect of different model crater age techniques. *Icarus*, 225(1), 173–184. https://doi.org/10.1016/j.icarus.2013.03.019
- Scott, E. R. D., & Fuller, M. (2004). A possible source for the Martian crustal magnetic field. Earth and Planetary Science Letters, 220(1), 83–90. https://doi.org/10.1016/S0012-821X(04)00032-9
- Shannon, C. E. (2001). A mathematical theory of communication. SIGMOBILE Mob. Comput. Commun. Rev., 5(1), 3–55. https://doi.org/10.1145/584091.584093
- Steele, S. C., Fu, R. R., Mittelholz, A., Ermakov, A. I., Citron, R. I., & Lillis, R. J. (2024). Weak magnetism of Martian impact basins may reflect cooling in a reversing dynamo. *Nature Communications*, 15(1), 6831. https://doi.org/10.1038/s41467-024-51092-4
- Steele, S. C., Fu, R. R., Volk, M. W., North, T. L., Brenner, A. R., Muxworthy, A. R., et al. (2023). Paleomagnetic evidence for a long-lived,
- potentially reversing martian dynamo at ~3.9 Ga. *Science Advances*, 9(21), eade9071. https://doi.org/10.1126/sciadv.ade9071
 Toft, P. B., Arkani-Hamed, J., & Haggerty, S. E. (1990). The effects of serpentinization on density and magnetic susceptibility: A petrophysical
- model. Physics of the Earth and Planetary Interiors, 65(1), 137–157. https://doi.org/10.1016/0031-9201(90)90082-9

 Uieda, L., Tian, D., Leong, W. J., Toney, L., Schlitzer, W., Grund, M., et al. (2021). PyGMT: A Python interface for the generic mapping tools.
- Venkatadri, T. K., & James, P. B. (2020). Variations of porosity in intermediate-sized lunar impact basins. *Icarus*, 352, 113953. https://doi.org/10.1016/j.icarus.2020.113953
- Vervelidou, F., Lesur, V., Grott, M., Morschhauser, A., & Lillis, R. J. (2017). Constraining the date of the martian dynamo shutdown by means of crater magnetization signatures. *Journal of Geophysical Research: Planets*, 122(11), 2294–2311. https://doi.org/10.1002/2017JE005410
- Wansing, A., Ebbing, J., & Moorkamp, M. (2024). The lithospheric structure of Greenland from a stepwise forward and inverse modelling approach. *Geophysical Journal International*, 238(2), 719–741. https://doi.org/10.1093/gji/ggae183
- Wieczorek, M. (2019). SHTools. Zenodo. https://doi.org/10.5281/zenodo.3457861
- Wieczorek, M. A. (2015). Gravity and topography of the terrestrial planets. *Planets and Moons*, 165–206. https://doi.org/10.1016/b978-044452748-6/00156-5
- Wieczorek, M. A., Broquet, A., McLennan, S. M., Rivoldini, A., Golombek, M., Antonangeli, D., et al. (2022). InSight constraints on the global character of the Martian crust. *Journal of Geophysical Research: Planets*, 127(5), e2022JE007298. https://doi.org/10.1029/2022JE007298
- Wiggins, S. E., Johnson, B. C., Collins, G. S., Jay Melosh, H., & Marchi, S. (2022). Widespread impact-generated porosity in early planetary crusts. *Nature Communications*, 13(1), 4817. https://doi.org/10.1038/s41467-022-32445-3
- Wordsworth, R., Knoll, A. H., Hurowitz, J., Baum, M., Ehlmann, B. L., Head, J. W., & Steakley, K. (2021). A coupled model of episodic warming, oxidation and geochemical transitions on early Mars. *Nature Geoscience*, 14(March), 127–132. https://doi.org/10.1038/s41561-021-00701-8
- Wörner, L., Root, B. C., Bouyer, P., Braxmaier, C., Dirkx, D., Encarnação, J., et al. (2023). MaQuIs—Concept for a Mars quantum gravity mission. *Planetary and Space Science*, 239, 105800. https://doi.org/10.1016/j.pss.2023.105800
- Wright, V., Morzfeld, M., & Manga, M. (2024). Liquid water in the Martian mid-crust. *Proceedings of the National Academy of Sciences*, 121(35), e2409983121. https://doi.org/10.1073/pnas.2409983121

MITTELHOLZ ET AL. 19 of 19